The American Journal of Human Genetics

Supplemental Data

Biallelic Mutations in Nuclear Pore Complex Subunit *NUP107* Cause Early-Childhood-Onset Steroid-Resistant Nephrotic Syndrome

Noriko Miyake, Hiroyasu Tsukaguchi, Eriko Koshimizu, Akemi Shono, Satoko Matsunaga, Masaaki Shiina, Yasuhiro Mimura, Shintaro Imamura, Tomonori Hirose, Koji Okudela, Kandai Nozu, Yuko Akioka, Motoshi Hattori, Norishige Yoshikawa, Akiko Kitamura, Hae Il Cheong, Shoji Kagami, Michiaki Yamashita, Atsushi Fujita, Satoko Miyatake, Yoshinori Tsurusaki, Mitsuko Nakashima, Hirotomo Saitsu, Kenichi Ohashi, Naoko Imamoto, Akihide Ryo, Kazuhiro Ogata, Kazumoto Iijima, and Naomichi Matsumoto

Supplemental Note: Case Reports

These unrelated families are all of Asian origin (four Japanese families, SRNS-1, SRNS-2, SRNS-TK1 and SRNS-TWH1; and one Korean family, SRNS-12) based on their clinical records and interviews (Fig. 1A). Previously, three families, SRNS-1, SRNS-2, SRNS-12, had been reported.[1] The affected individuals show only a kidney-specific phenotype with no abnormal manifestations of other organs, including neurological and sensory features.

SRNS-1

In this family, the older sister (II-2) showed proteinuria at 3 years of age and was treated with steroids. A renal biopsy showed focal glomerulosclerosis of a not-otherwise-specific (NOS) subtype. She died from a varicella zoster virus infection at 3 years of age, before reaching ESRD. The youngest brother (II-4) first developed proteinuria at 3 years, similarly to his affected sister. He received steroid therapy combined with immunosuppressants (cyclosporine [CyA] and cyclophosphamide [CPA]). However, his renal function progressively worsened and he became dialysis-dependent at 9 years of age. He received a renal transplant from his father at 11 years of age and no recurrence of SRNS to date. Parents (I-1, I-2) and two siblings (II-1, II-3) have shown no renal symptoms.

SRNS-2

The extended SRNS family was first recognized by early-onset nephrotic syndrome in the older sister (II-1), who was found to have proteinuria at 2 years of age. She was treated with steroids combined with CyA.

However, she was resistant to drug therapy and progressed to ESRD by age 10 years. The histology of her first renal biopsy at 2 years old showed minimal change but her second biopsy at 4 years revealed FSGS (NOS subtype). At age 10, she underwent a renal transplant of a kidney donated from her father. Subsequently, her two younger identical-twin brothers (II-3 and II-4) displayed early onset SRNS, with a clinical course quite similar that of the older sister (II-1). One brother (II-3) first manifested SRNS at age 2 years. He reached ESRD at 7 years, and received a renal transplant from his mother at that age. The other brother (II-4) took a similar clinical course to his affected siblings, developing SRNS at 2 years and progressing to ESRD at 7 years. He received a cadaveric renal transplantation from his paternal grandmother at 9 years. In all three affected individuals, no post-transplant recurrence of SRNS has been observed.

SRNS-TK1

The first child (II-1) developed nephrotic syndrome at age of 2 years. He was resistant to the standard steroid regimen with CyA and progressed to ESRS at age of 4 years. His renal biopsy at 2 years revealed FSGS. His parents (I-1, I-2) and one brother (II-2) were healthy and had no renal abnormalities. He received a renal transplant at age 7 years from his father, and did not show any recurrence of SRNS.

SRNS-TWH1

The elder sister (II-1) first manifested nephrotic syndrome at 3 years of age. Her renal biopsy revealed a collapsing subtype of FSGS. Despite combination therapy with steroids, angiotensin II receptor blocker (ARB), and plasmapheresis, she rapidly progressed to ESRD at age 4 years. She received a transplanted kidney from her father (I-1). Her younger brother (II-2) exhibited early-onset SRNS quite similar to his

affected sister: He developed a nephrotic condition by age 3 years and received combined immunosuppressive therapy (steroid, CyA and ARB). However, he was resistant to the therapy and had developed ESRD by age 5 years. His renal pathology at age 3 years was a collapsing subtype of FSGS. He is currently treated by peritoneal dialysis, waiting for renal transplantation.

SRNS-12

This SRNS family has been previously reported.[1] The third daughter (II-3; proband) first manifested nephrotic syndrome at the age of 11 years. Her renal biopsy revealed NOS subtype of FSGS. Despite combined therapy with steroids and ARB, she rapidly progressed to ESRD by age 12 years and thereafter started peritoneal dialysis. She received a kidney transplant from her father at age 14 years. She has not developed NS in the 10 years since her kidney transplantation.

The second daughter (II-2) developed proteinuria at age 10 years. However, her clinical course was milder than that of her younger sister, the third daughter (II-3) who reached ESRD only 1 year after the onset of SRNS. She has never produced nephrotic proteinuria, nor received immunosuppressive therapy. Her subnephrotic-range proteinuria (1.4–4.0 g per gram creatinine) has persisted over the last 10 years. Renal biopsy has not yet been performed. Her renal function has been preserved compared to her younger sister (II-3), but has gradually declined from eGFR 85.5 ml/min (at age 32 years) to 62.2 ml/min (at her current age of 34 years) under administration of ARB alone (losartan 50 mg/day). The parents (I-1, I-2) and eldest daughter (II-1) have not shown any renal symptoms.

Figure S1

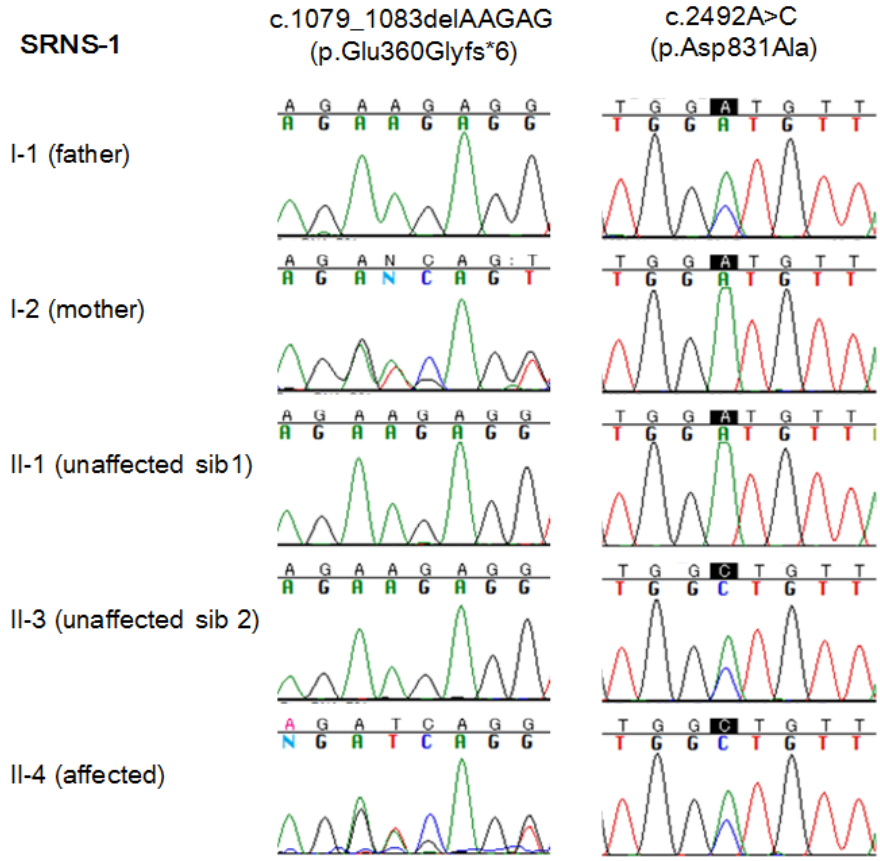
SRNS-1
c.1079_1083delAAGAG
(p.Glu360Glyfs*6)
c.2492A>C
(p.Asp831Ala)
I-1 (father)
I-2 (mother)
II-1 (unaffected sib1)
II-3 (unaffected sib 2)
II-4 (affected)

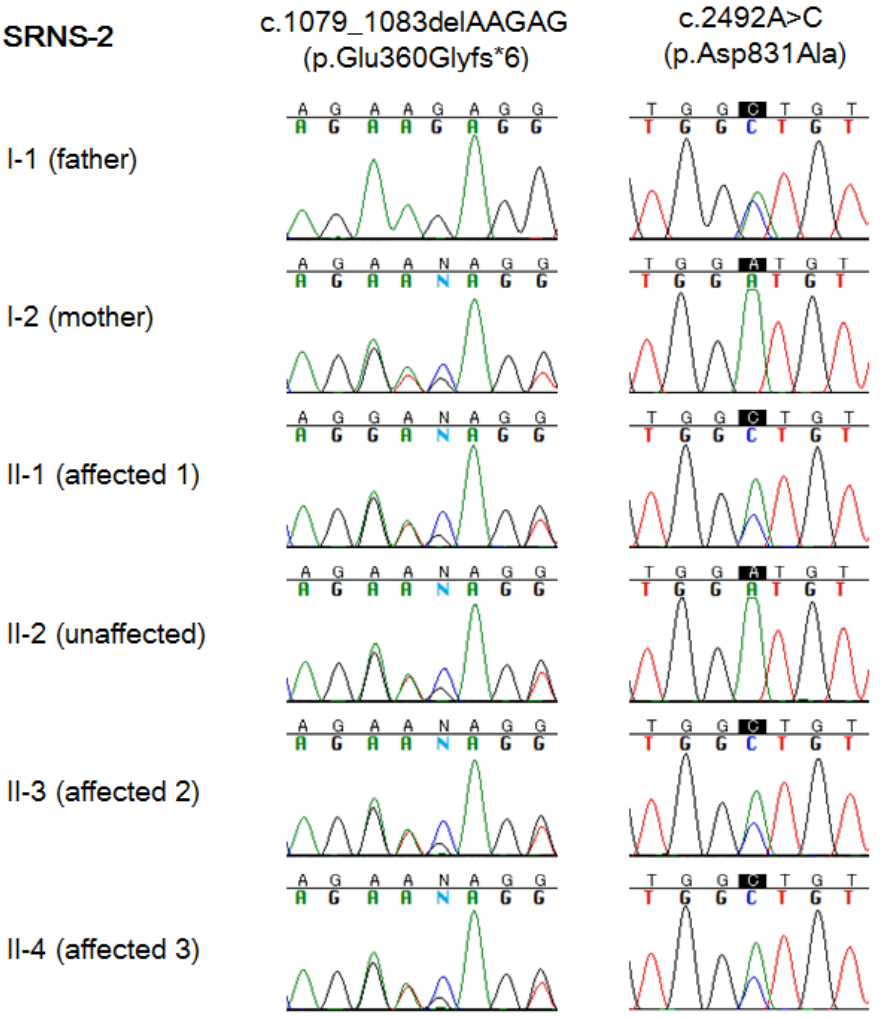
SRNS-2
c.1079_1083delAAGAG
(p.Glu360Glyfs*6)
c.2492A>C
(p.Asp831Ala)
I-1 (father)
I-2 (mother)
II-1 (affected 1)
II-2 (unaffected)
II-3 (affected 2)
II-4 (affected 3)

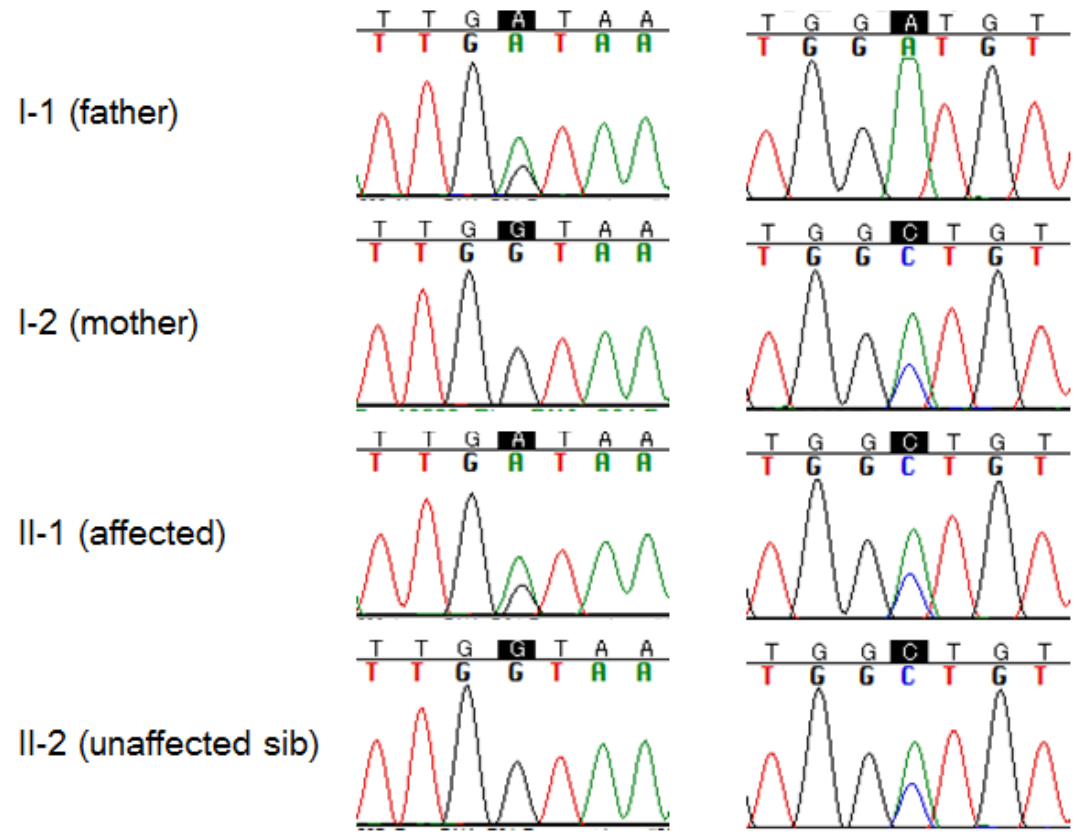
SRNS-TK1
c.969+1G>A
c.2492A>C
(p.Asp831Ala)
I-1 (father)
I-2 (mother)
II-1 (affected)
II-2 (unaffected sib)

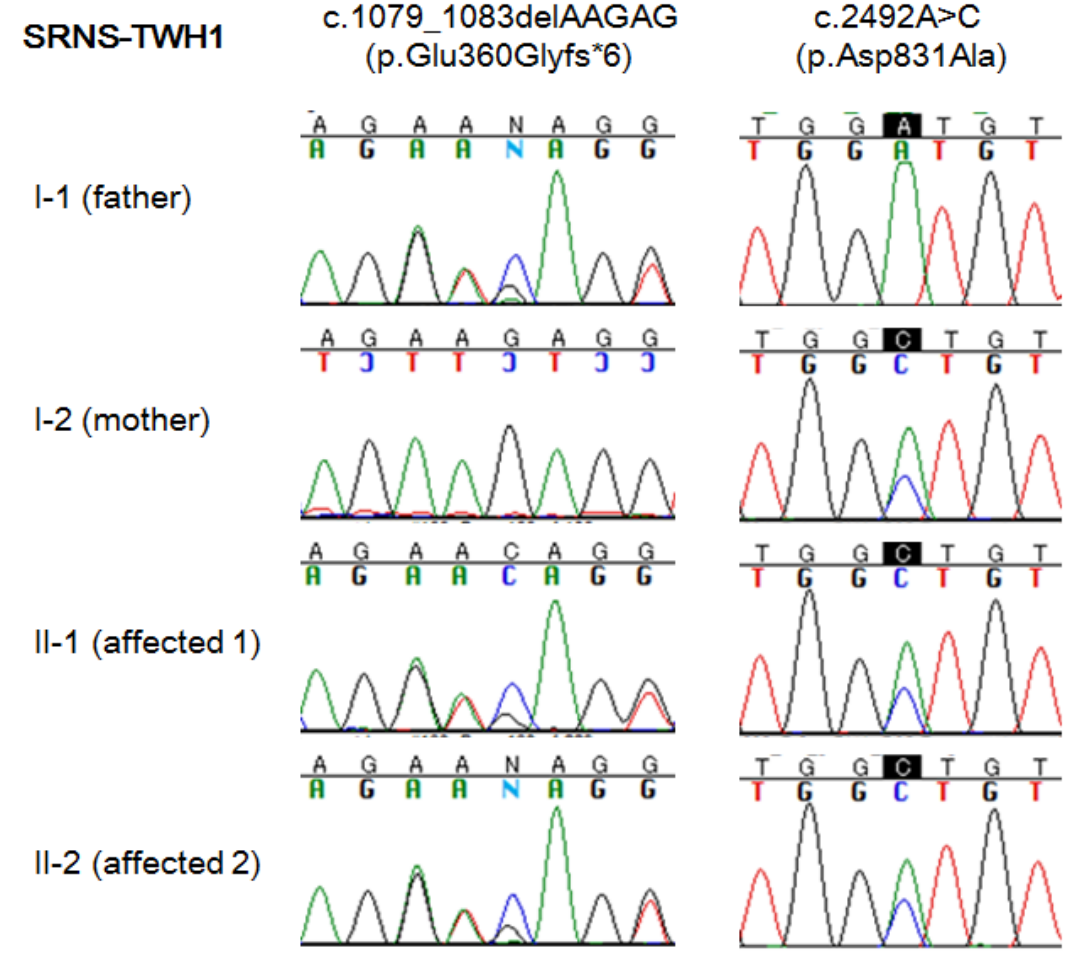
SRNS-TWH1
c.1079_1083delAAGAG
(p.Glu360Glyfs*6)
c.2492A>C
(p.Asp831Ala)
I-1 (father)
I-2 (mother)
II-1 (affected 1)
II-2 (affected 2)

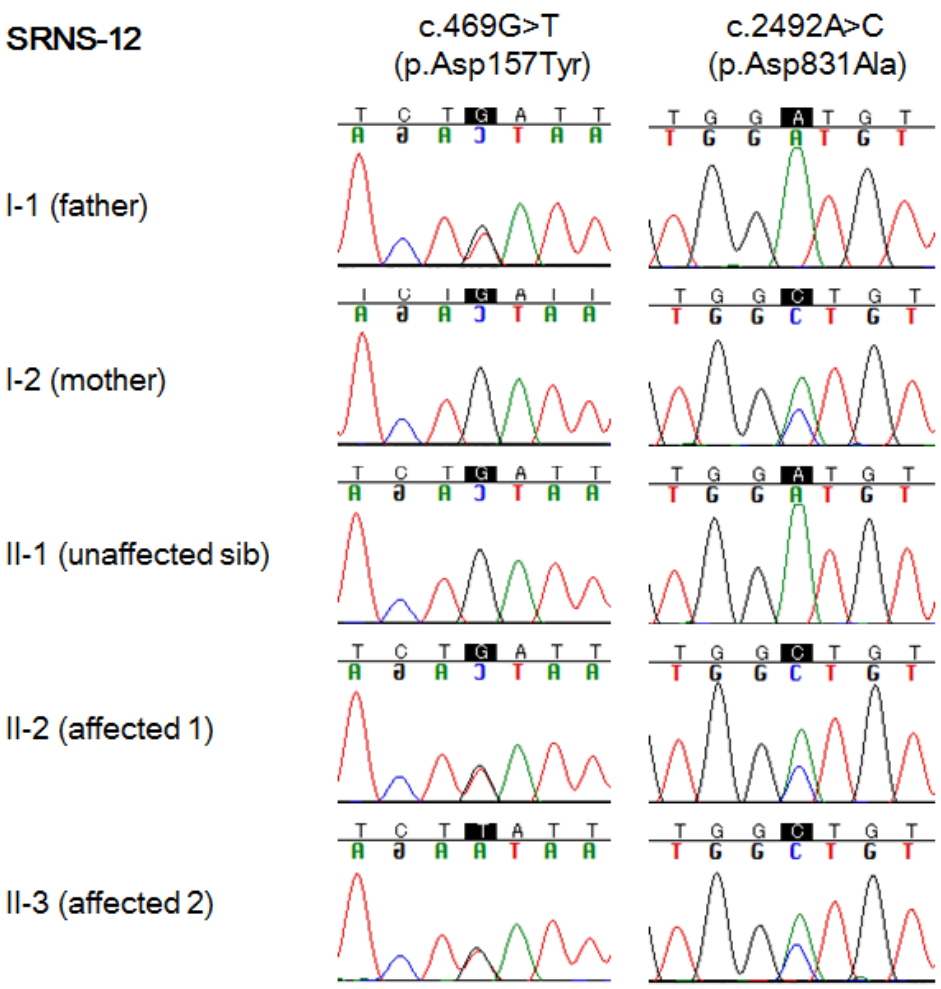

Figure S1. Electropherograms of *NUP107* Mutations Found in Families with Early-Onset Steroid-Resistant Nephrotic Syndrome

Compound heterozygous mutations co-segregated completely with all the affected individuals in the five families.

Figure S2

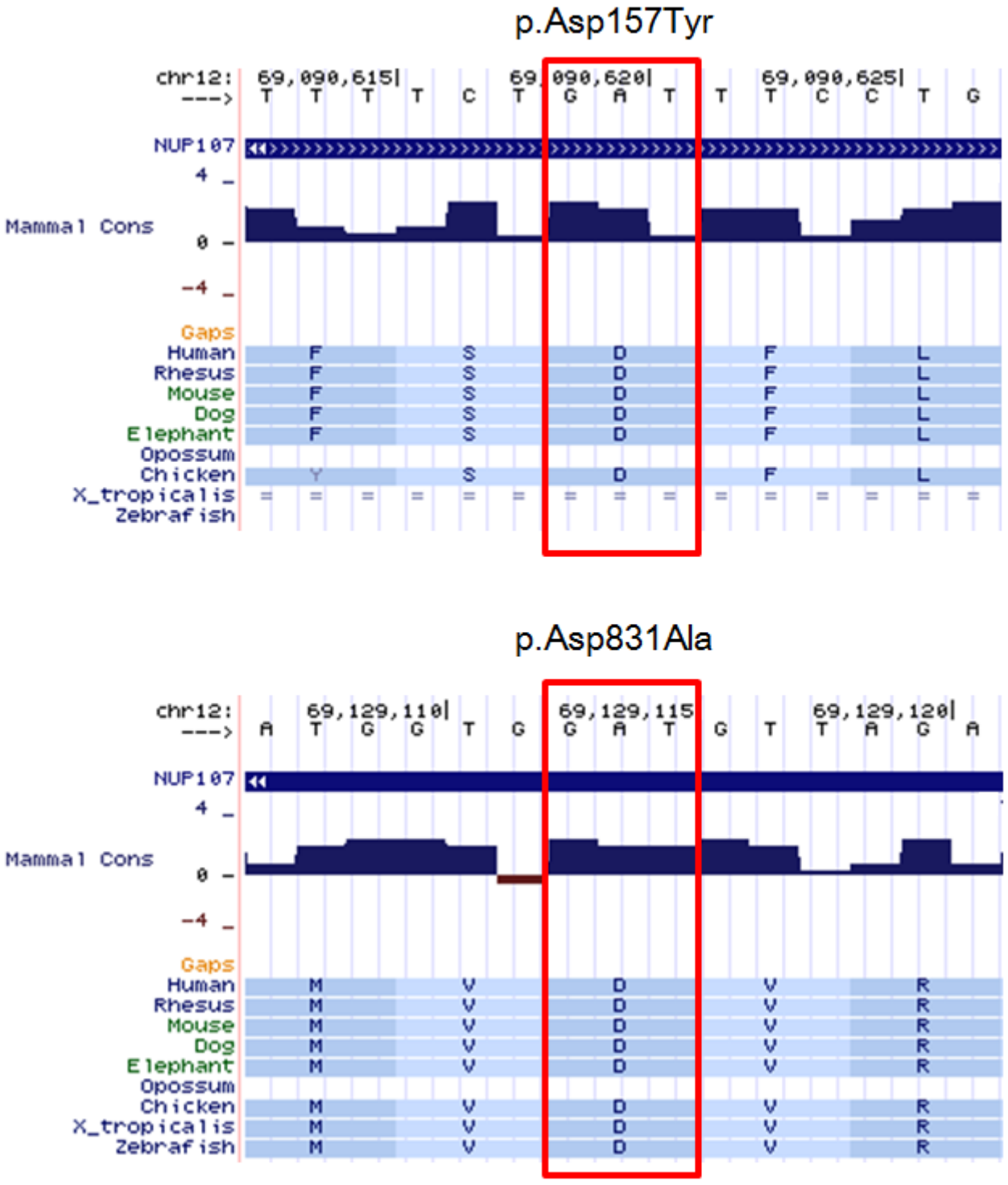

Figure S2. Evolutionary Conservation of the Amino Acids Altered by Two Missense Mutations

The amino acids altered in the affected individuals are evolutionally conserved from chickens to humans (p.Asp157) and from zebrafish to humans (p.Asp831).

Figure S3

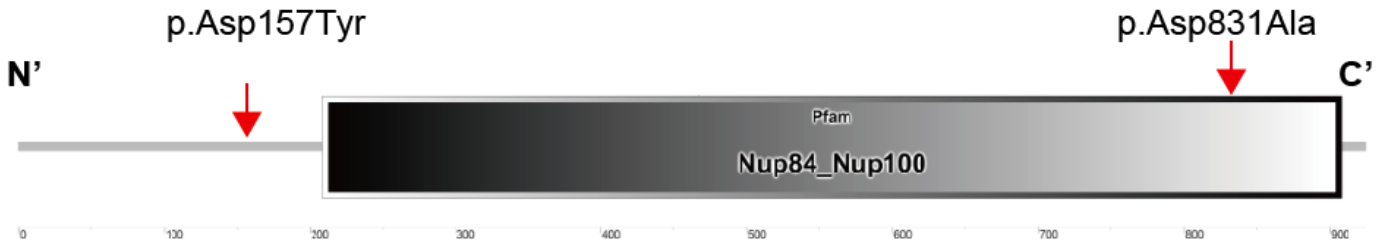

Figure S3. Locations of the Two Missense Mutations in NUP107

The region from 209 to 908 amino acids was defined as the Nup84_Nup100 domain by the SMART program (http://smart.embl-heidelberg.de/) using NUP107 protein sequence (NP_065134). p.Asp831Ala is localized within this domain.

Figure S4

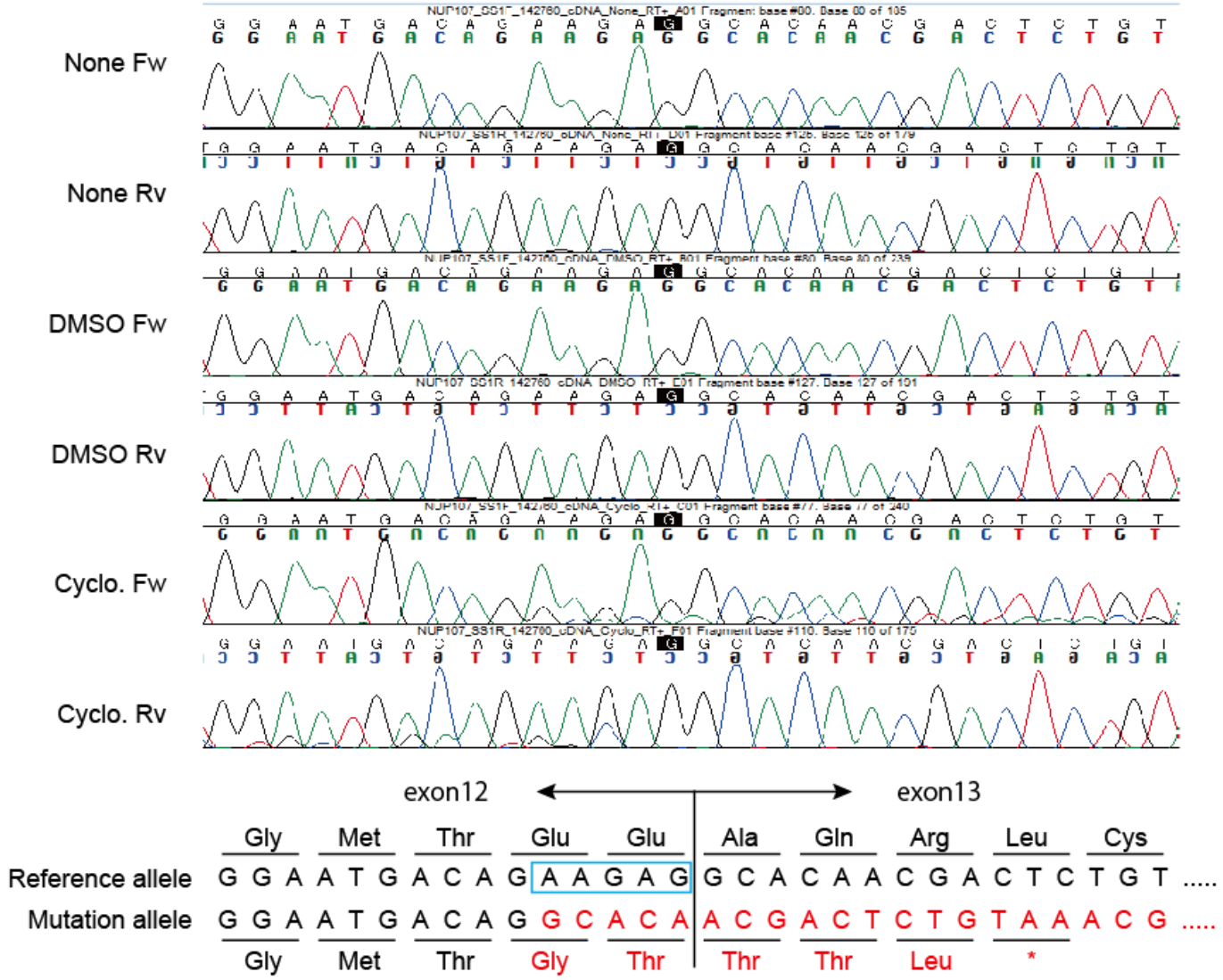

Figure S4. Nonsense Mediated mRNA Decay by the 5-bp Deletion (c.1079_1083delAAGAG)

These chromatograms are from SRNS-TWH II-2. The 5-bp deletion (marked by the blue box) resulted in nonsense-mediated mRNA decay of the mutant allele as the cDNA sequence of the mutant allele can be seen only after treatment with cycloheximide.

Figure S5

[Splice site prediction by Neural Network]

Donor site predictions for WT :

Start	End	Score	Exon	Intron
710	724	0.57	ggctgca	gtgagtca
1202	1216	0.80	tgaattg	gtaaatgt
1302	1316	0.80	tctaaag	gtttgcac
1392	1406	0.91	ttgaatt	gtaagtaa
1485	1499	0.70	atataag	gtagtgac
1558	1572	0.93	gtttgag	gttagaac

Donor site predictions for Mut :

Start	End	Score	Exon	Intron
710	724	0.57	ggctgca	gtgagtca
1302	1316	0.80	tctaaag	gtttgcac
1392	1406	0.91	ttgaatt	gtaagtaa
1485	1499	0.70	atataag	gtagtgac
1558	1572	0.93	gtttgag	gttagaac

[NetGene2 v. 2.4]

WT

```
Donor splice sites, direct strand
---------------------------------
                pos 5'->3'  phase strand  confidence  5'      exon intron    3'
                   1209        0      +        0.42        CACTGAATTG^GTAAATGTTC
                   1399        2      +        0.32        CCTTTGAATT^GTAAGTAATA
                   1565        0      +        0.00        TTGGTTTGAG^GTTAGAACGG
```

Mut

```
Donor splice sites, direct strand
---------------------------------
                pos 5'->3'  phase strand  confidence  5'      exon intron    3'
                   1399        2      +        0.32        CCTTTGAATT^GTAAGTAATA
                   1565        0      +        0.00        TTGGTTTGAG^GTTAGAACGG
```

Figure S5. *In silico* Prediction of the Splicing Abnormality Caused by c.969+1G>A

The upper and lower panels show the splice sites predicted by NNSPLICE 0.9 (http://www.fruitfly.org/seq_tools/splice.html) and NetGene2 v. 2.4 (http://www.cbs.dtu.dk/services/NetGene2/), respectively. The canonical donor site in the wild-type allele marked by red boxes (based on the two prediction programs) is abolished in the mutant allele.

Figure S6

					SRNS-1	SRNS-2	SRNS-TK1	SRNS-TWH1	SRNS-12
#CHROM	POS	ID	REF	ALT	II-4	II-1	II-1	II-1	II-3
12	66838243	rs10878422	A	G	G	G	G	G	G
12	67706466	rs1060350	G	A	G	G	G	G	G
12	68045403	rs10878641	G	A	A	A	G	G	A
12	68052178	rs3741644	G	T	T	(T)	T	T	T
12	68372071	rs7299287	C	A	A	(A)	A	A	(A)
12	68595719	rs10748100	T	C	T	C	T	T	(T)
12	68595787	rs10748101	A	G	A	G	A	A	(A)
12	68646521	rs2227491	T	C	T	C	T	T	(T)
12	68688939	rs7958232	C	T	T	(T)	T	T	(T)
12	68707576	rs4575357	G	A	A	(A)	A	A	G
12	68708761	rs2306393	C	T	T	(T)	T	T	(T)
12	68719216	rs2870812	G	A	A	(A)	A	A	(A)
12	68720627	rs962976	G	A	A	(A)	A	A	(A)
12	68721040	rs962977	A	G	G	(G)	G	G	(G)
12	68724951	rs3741808	G	T	T	(T)	T	T	(T)
12	68867496	.	T	TA	TA	TA	TA	TA	TA
12	68868056	rs9325188	A	G	G	G	G	G	G
12	68868289	rs2015278	G	A	A	A	A	A	A
12	68881347	rs7307851	C	G	G	G	G	G	G
12	68881563	.	TC	T	T	T	T	T	T
12	69129114	c.2492A>C	A	C	C	C	C	C	C
12	69207162	rs1470383	G	A	A	A	A	A	A
12	69208578	rs1846402	A	C	C	C	C	C	C
12	69218038	rs2291857	T	G	G	G	G	G	G
12	69250548	rs3741598	C	T	T	T	T	T	T
12	69261044	rs1144949	C	T	T	T	T	T	T
12	69279736	rs2701085	A	G	G	G	G	G	G
12	69633379	rs2305642	A	G	G	G	G	G	(G)
12	69645864	rs490872	A	G	G	G	G	G	(G)
12	69646010	rs607797	T	C	C	C	C	C	(C)
12	69652336	.	G	GT	GT	GT	GT	GT	(GT)
12	69653146	rs2231700	T	C	C	C	C	C	(C)
12	69667075	rs1463335	T	A	A	A	A	A	(A)
12	69678311	.	T	C	C	C	C	C	C
12	69747177	rs710794	C	T	T	T	T	T	T
12	69753595	rs622656	C	T	C	T	C	T	C
12	69759551	.	AT	A	AT	A	AT	A	AT
12	69967636	rs512853	C	T	T	T	T	T	T
12	69979127	rs17106752	G	A	G	A	G	G	(G)
12	69980028	rs485288	G	A	A	A	A	A	A
12	69980141	rs484319	G	C	C	C	C	C	C
12	69980434	rs80262100	C	T	C	T	C	C	(C)
12	69981862	rs530701	G	A	A	A	A	A	A
12	69987494	rs710773	G	A	A	A	A	A	A
12	69991627	rs710765	C	T	T	T	T	T	T
12	69991675	rs35639	T	C	T	C	T	T	(T)
12	70070942	rs710718	A	G	G	G	G	G	G
12	70078124	rs710715	G	C	C	C	C	G	C
12	70078172	rs710714	C	T	T	T	T	C	T
12	70088085	.	AGT	A	AGT	A	AGT	AGT	AGT
12	70091432	rs775429	T	C	C	C	C	C	C
12	70190408	rs17120917	A	C	C	(C)	A	A	A
12	70273303	rs1240286	C	G	G	G	G	G	G
12	70274160	.	G	A	A	A	A	A	A

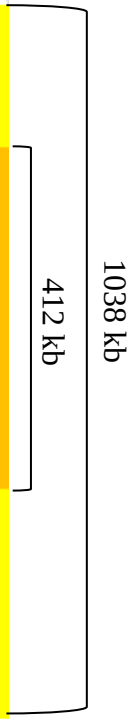

Figure S6. A Common Haplotype That Harbors c.2492A>C (p.Asp831Ala) Was Found in the Five SRNS Families

The confirmed mutation-specific haplotype (412 kb in size) highlighted in orange is common to all the families. The yellow highlighted region together with orange highlighted region (1038 kb in size) could be

considered the common haplotype if the inferred SNPs within parentheses are included, as parental exome data were unavailable for SRNS-2 and SRNS-12.

Figure S7

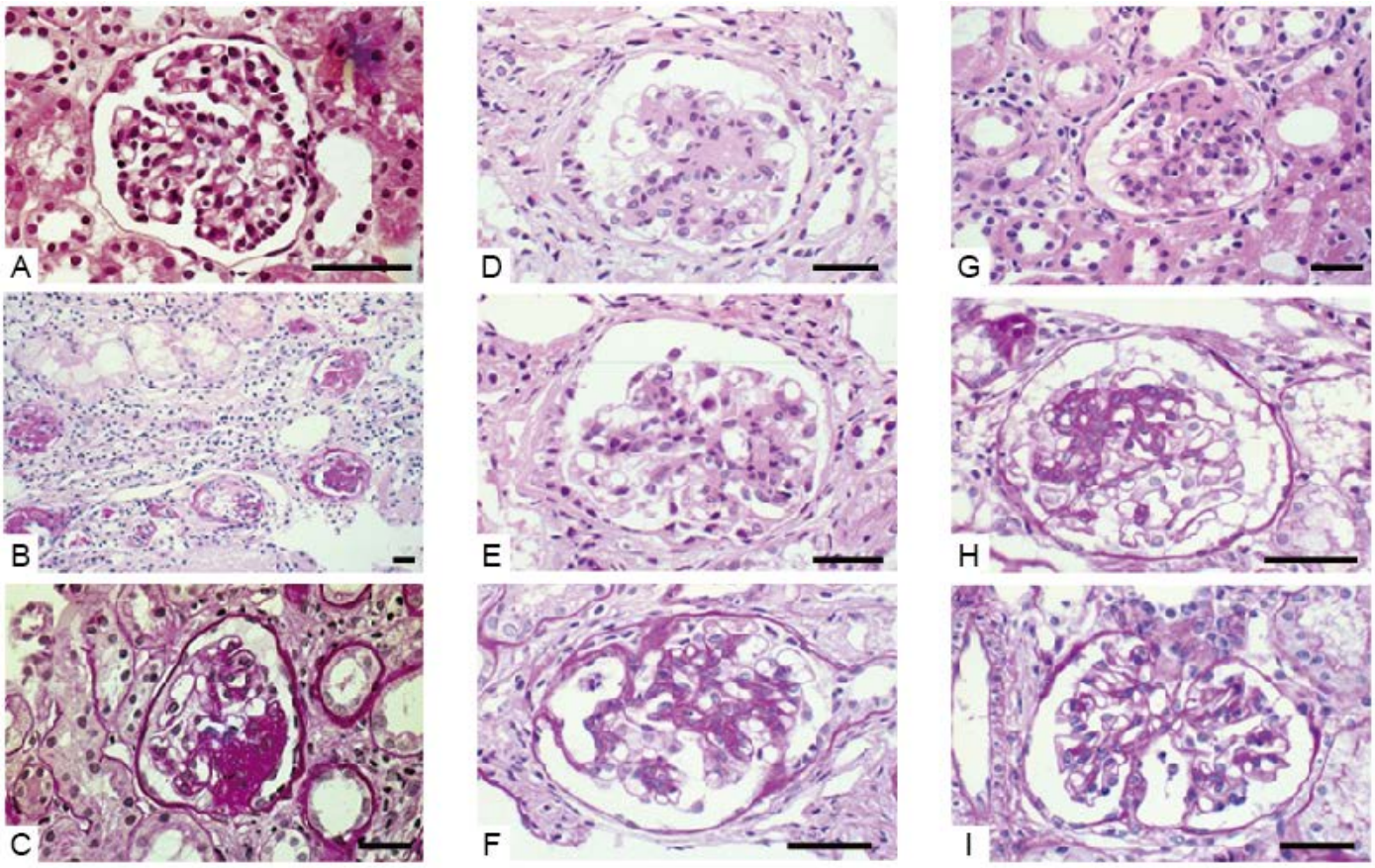

Figure S7. Histopathological Images of Renal Biopsies from Affected Individuals in the SRNS-2 Family

SRNS-2 II-1 underwent renal biopsies at ages 2 years (A) and at 4 years (B, C). The sclerotic changes became more prominent at 4 years of age. Biopsied samples of SRNS-2 II-3 (D, E, F) and SRNS-2 II-4 (G, H, I) stained with periodic Acid Schiff show focal segmental glomerulosclerosis [image magnifications: ×100 (b), ×400 (a, c–i)]. Scale bars: 40 μm.

Figure S8

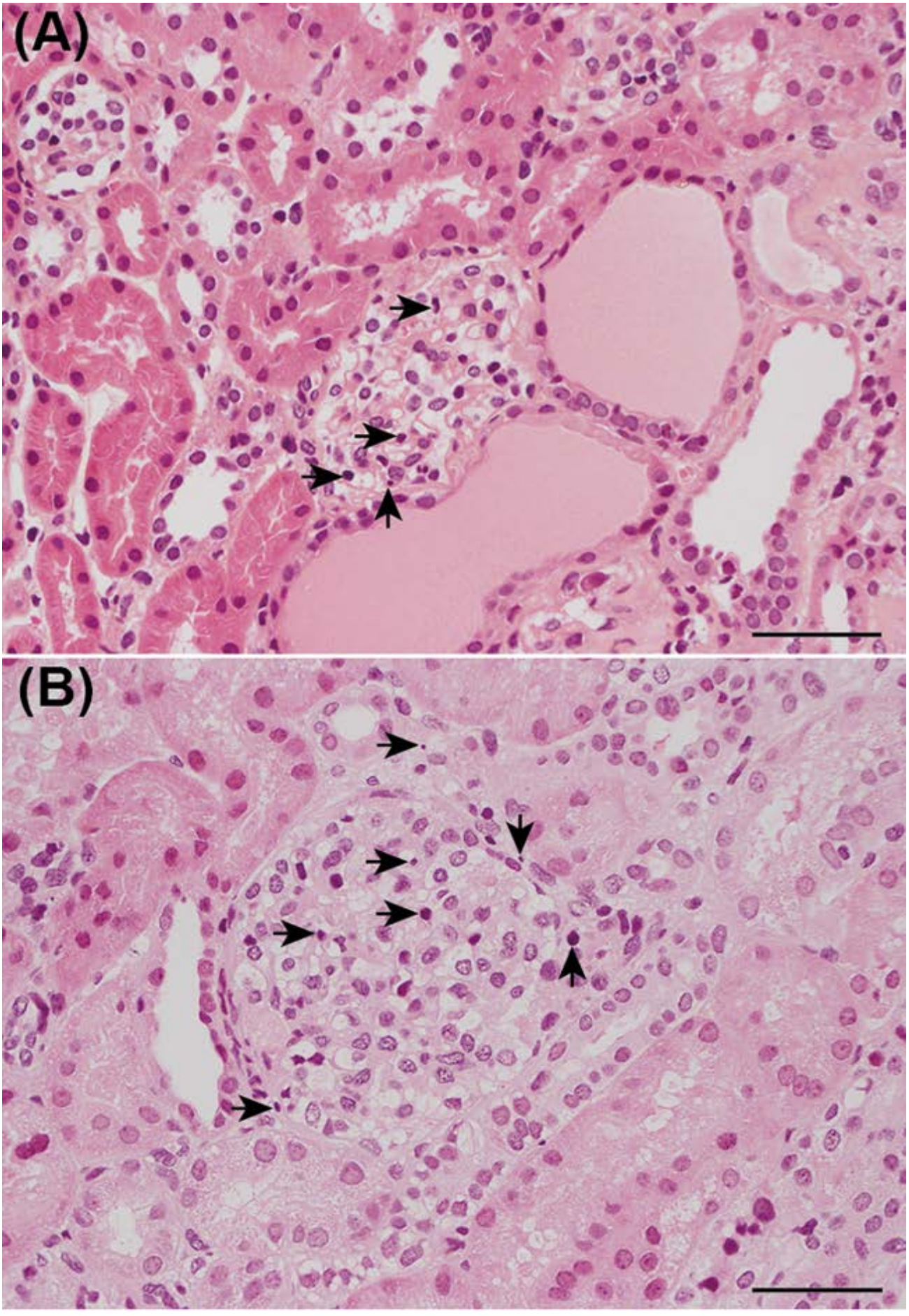

Figure S8. Hematoxylin and Eosin-Stained Kidney Tissues from Affected Individuals in the

SRNS-TWH1 Family

These images are from SRNS-TWH1 II-1 (A) and SRNS-TWH1 II-2 (B). Cells that showed nuclear shrinkage and fragmentation were occasionally found in the glomeruli and renal tubules (arrows). Scale bars: 50 μm.

Figure S9

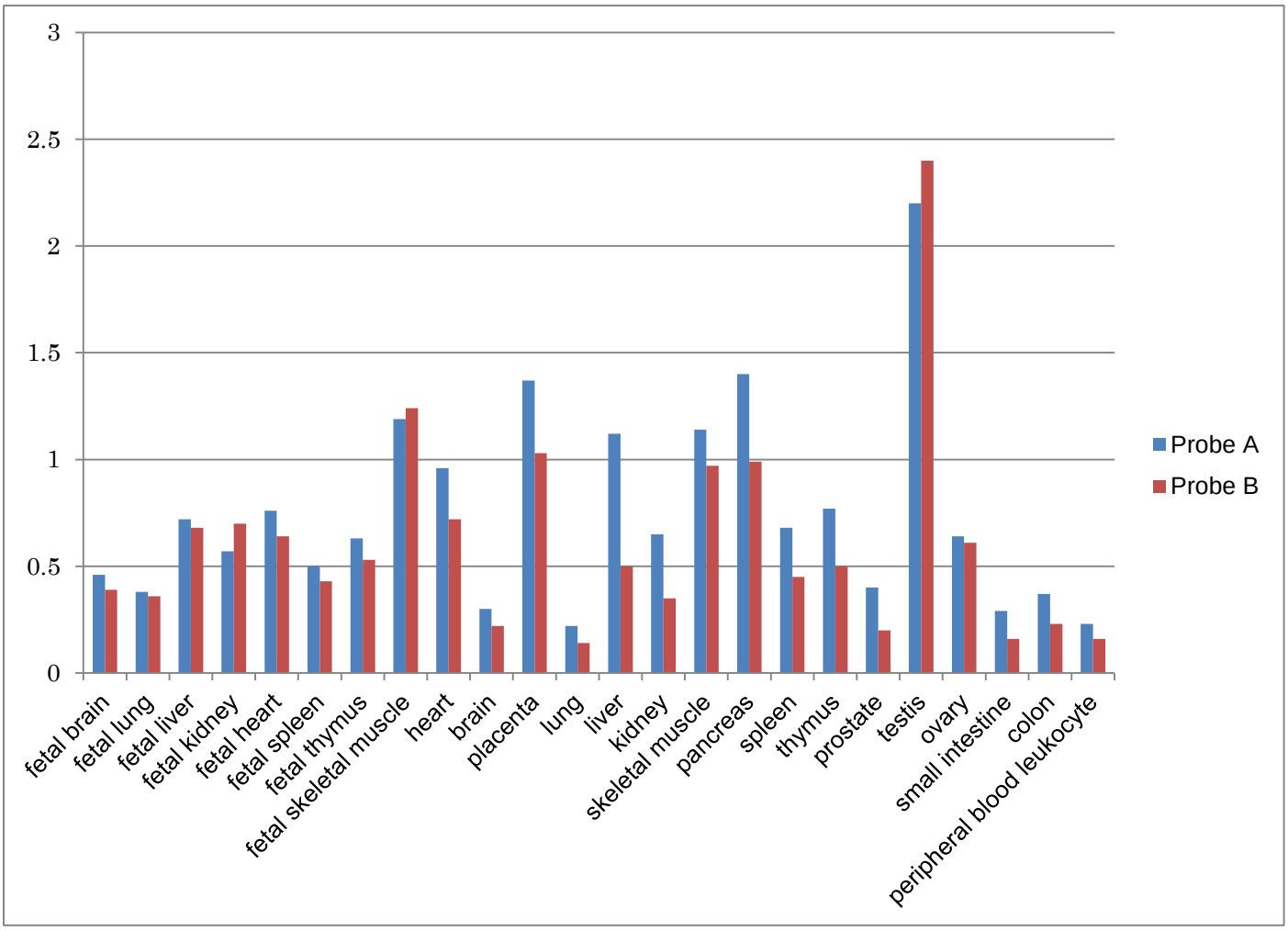

Figure S9. Quantitative *NUP107* Expression Analysis in Fetal and Adult Tissues Using TaqMan Assays

TaqMan Probes A (Hs00914854_g1) and B (Hs00220703_m1) show similar *NUP107* expression levels in various tissues. The Y-axis represents the relative expression levels normalized against beta-actin expression levels.

Figure S10

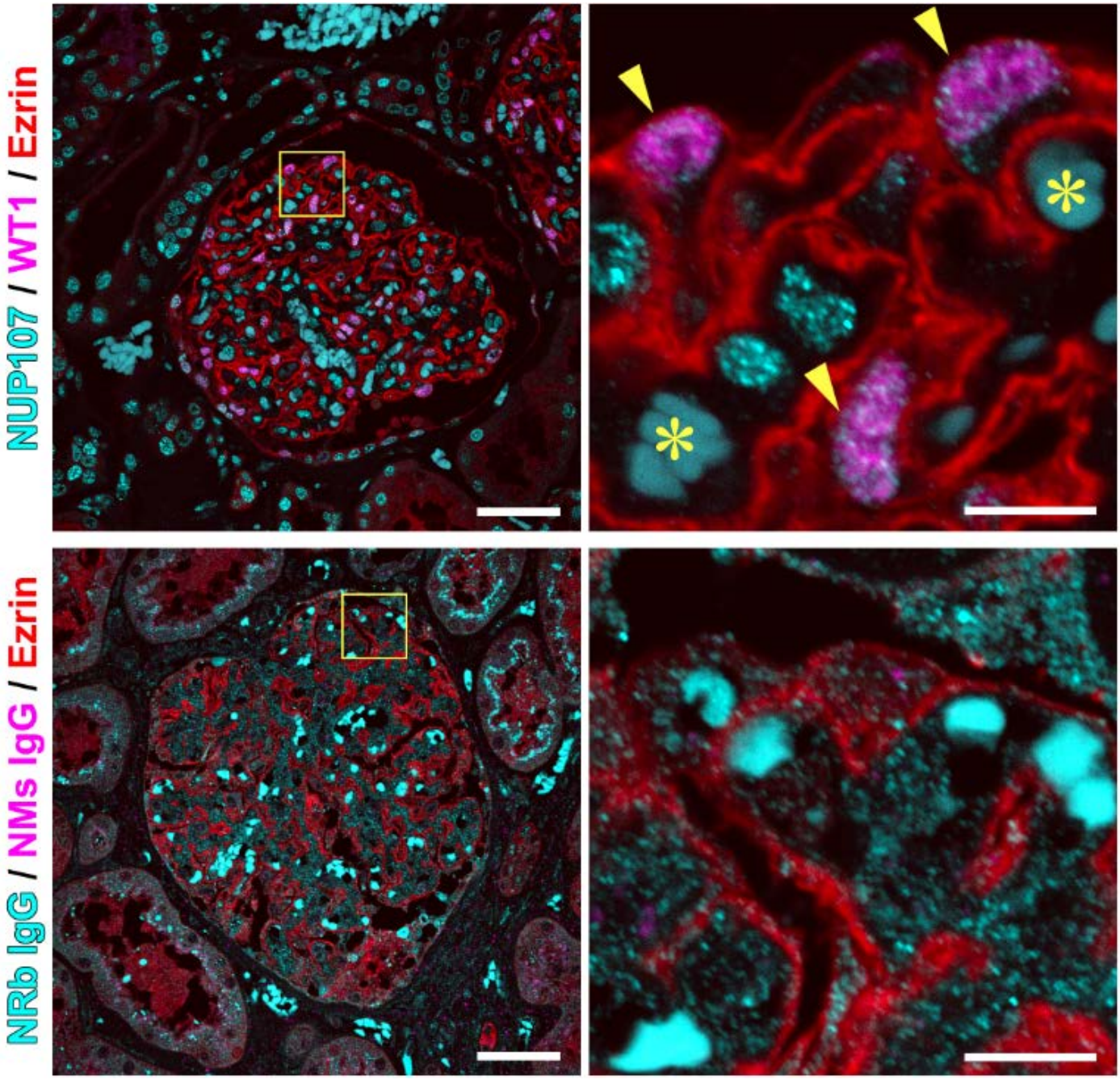

Figure S10. Nuclear localization of NUP107 in podocytes

Podocytes in human kidney sections were identified using antibodies against WT1 (magenta) and Ezrin (red) (upper panels). Boxed regions are enlarged (right) to show the speckle-like nuclear distribution of NUP107 in more detail. A single optical section shows the glomerular capillary tufts to be covered with podocytes; their nuclei on the glomeruli surfaces contain WT1 and NUP107 (arrow heads). Asterisks: autofluorescent

erythrocytes in the capillary lumen. Normal rabbit IgG (NRb IgG) and normal mouse IgG (NMs IgG) were used for negative controls (lower panels). Scale bars: 50 μm (left); 10 μm (right).

Figure S11

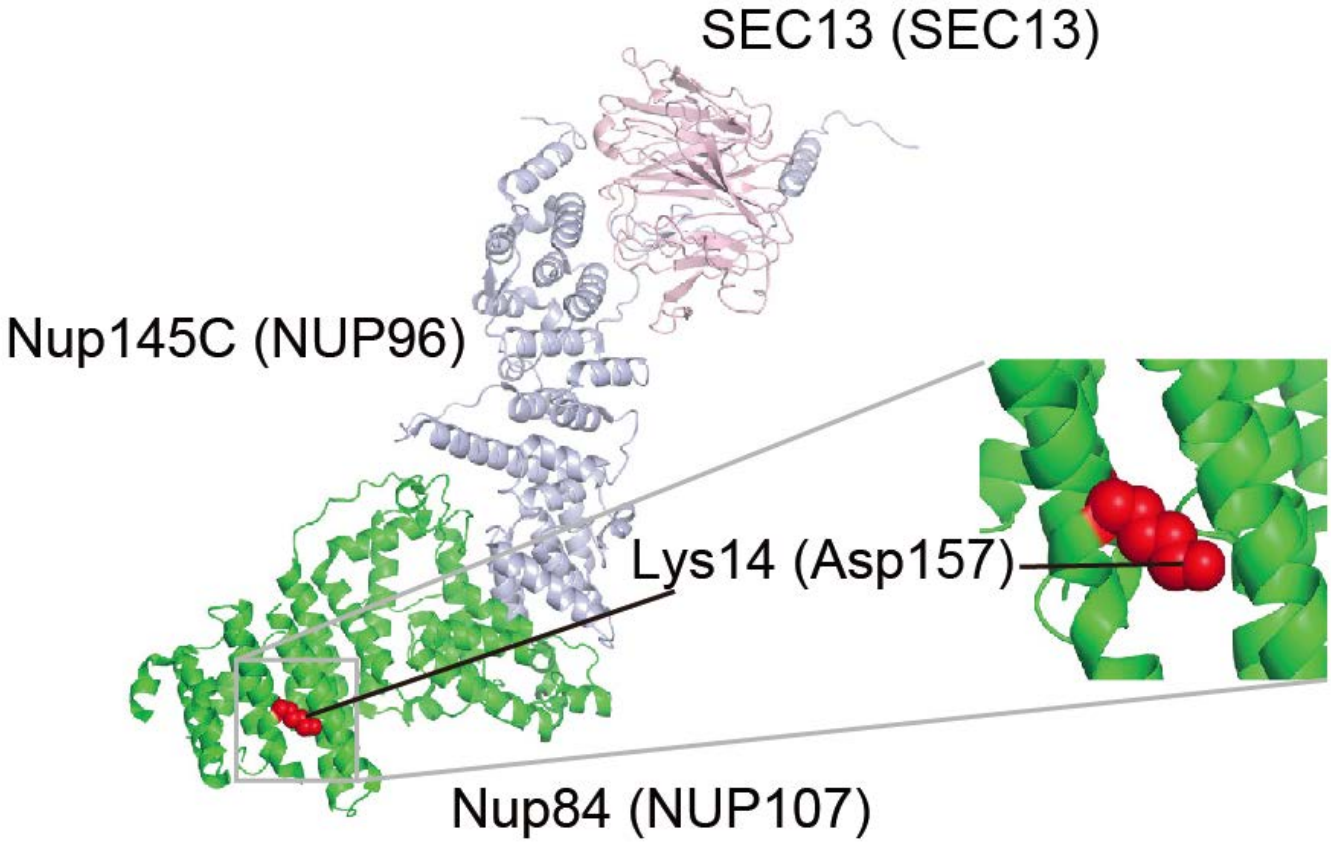

Figure S11. Location of the p.Asp157 Missense Substitution

Crystal structure of yeast Sec13 (amino acid residues 1–297, light pink)-Nup145C (731–1158, light blue)-Nup84 (1–460, green) complex (PDB code; 3IKO) is shown with a magnified view around the variant site in Nup84, which is the yeast homolog of human NUP107. Each component of the complex is annotated with the corresponding human homologs in parentheses. Lys 14 of yeast Nup84 (Asp 157 of human NUP107) is colored red; its side chain is shown as a van der Waals representation.

Figure S12

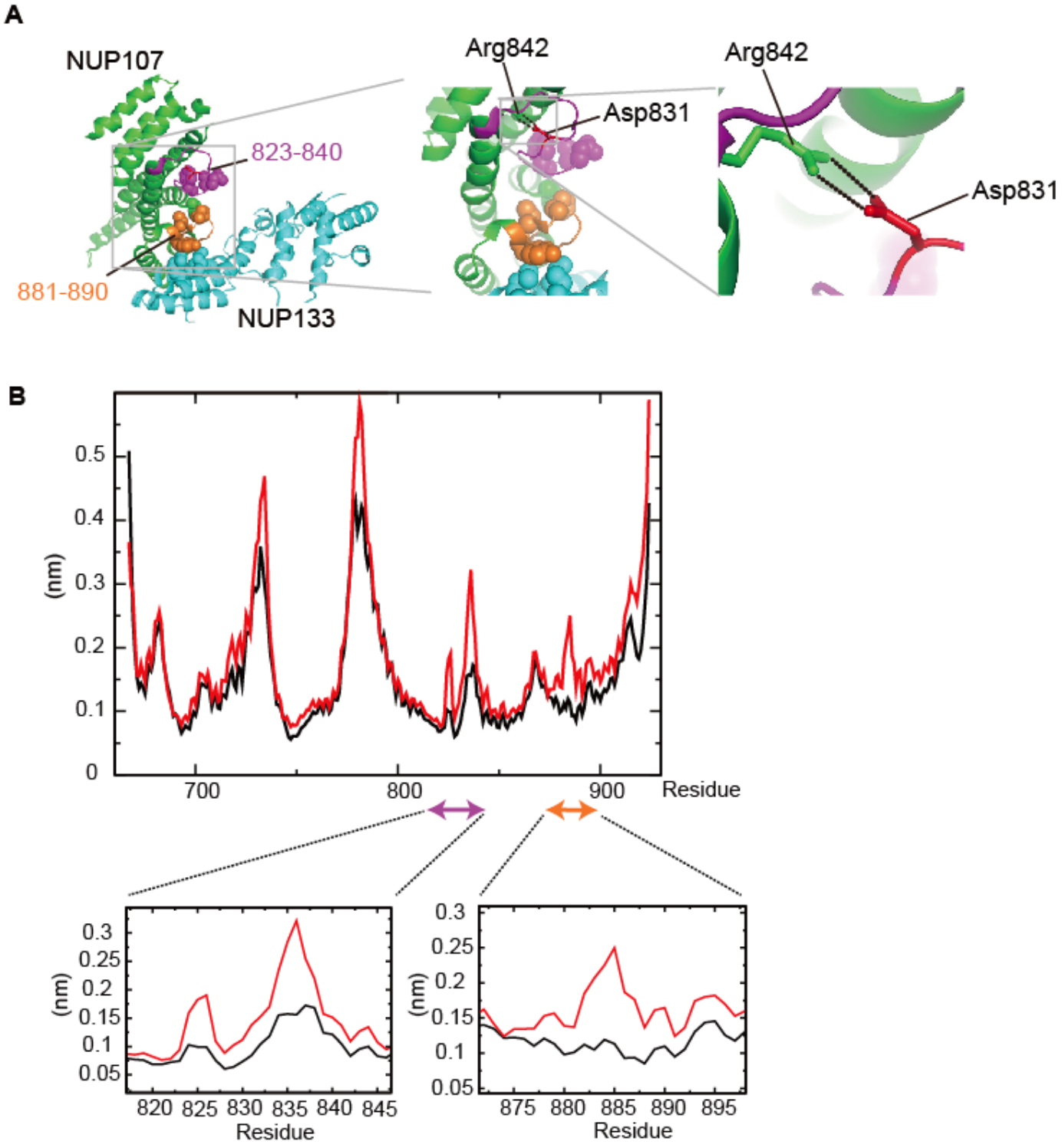

Figure S12. Molecular Structure Effects Caused by Replacement of Residue Asp831 in NUP107

(A) Crystal structure of the nucleoporin NUP107-NUP133 complex (PDB code 3CQC), which includes the human NUP107 fragment (containing an amino acid region at 658–925, in green except for the regions described below), and the human NUP133 fragment (containing the amino acid region 935–1156, in cyan),

which is shown with magnified views of the squared regions. A residue at the mutation site, Asp 831 (in red), and amino acid regions 823–840 (in magenta) and 881–890 (in orange), are predicted by the molecular dynamics simulation to cause a structural perturbation of the p.Asp831Ala mutation (see main text). Side chains of some hydrophobic residues that are involved in these two regions are shown in a van der Waals sphere representation; those of Asp 831 and Arg 842 are depicted as sticks. Black dotted lines represent hydrogen bonds. (B) Root mean squared fluctuation (RMSF) plots of NUP107 along the MD simulations. The RMSFs of the backbone atoms of the wild-type NUP107 fragment (amino acid residues 685–925; in black) and its Asp831Ala variant (red) are plotted. Graphic scales corresponding to amino acid regions 815–847 and 873–897 are magnified.

Figure S13

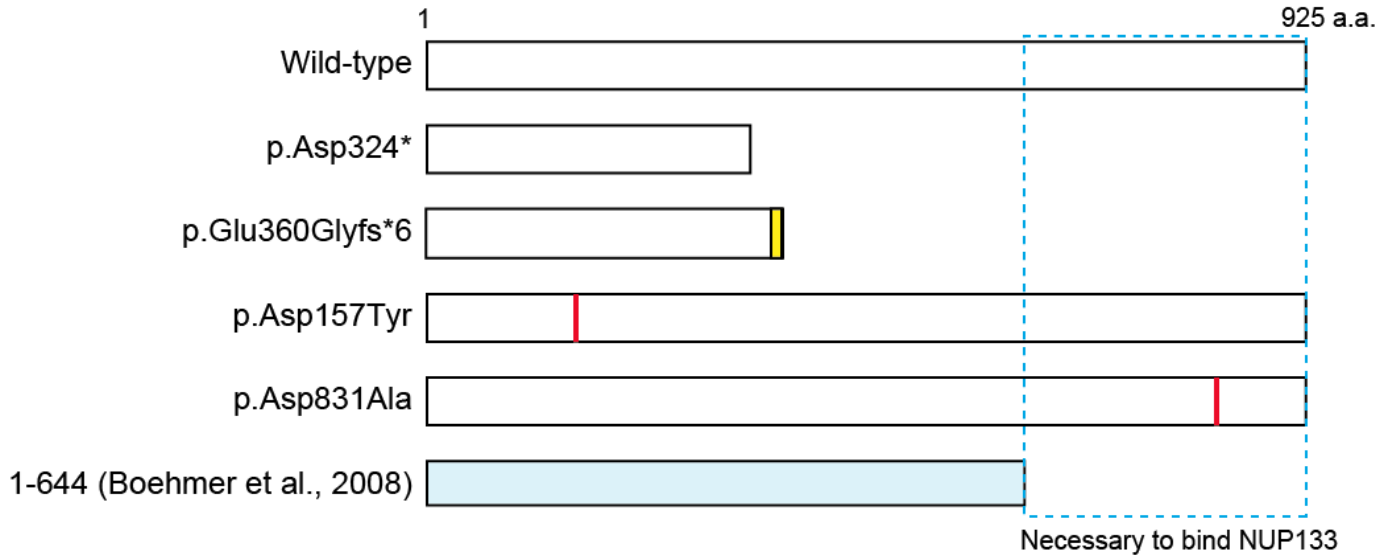

Figure S13. Schematic of the NUP107 Constructs Illustrating the Mutation Positions

Wild-type and four mutant *NUP107* constructs were subcloned into a mammalian expression vector. The shorter protein (light blue box, 1–644 amino acids) cannot bind to NUP133.[2] The blue dotted rectangular region is important for binding to NUP133.[2] The yellow box and red vertical bars indicate the positions of added abnormal amino acids by the frameshift mutation and the positions of each point mutation, respectively.

Figure S14

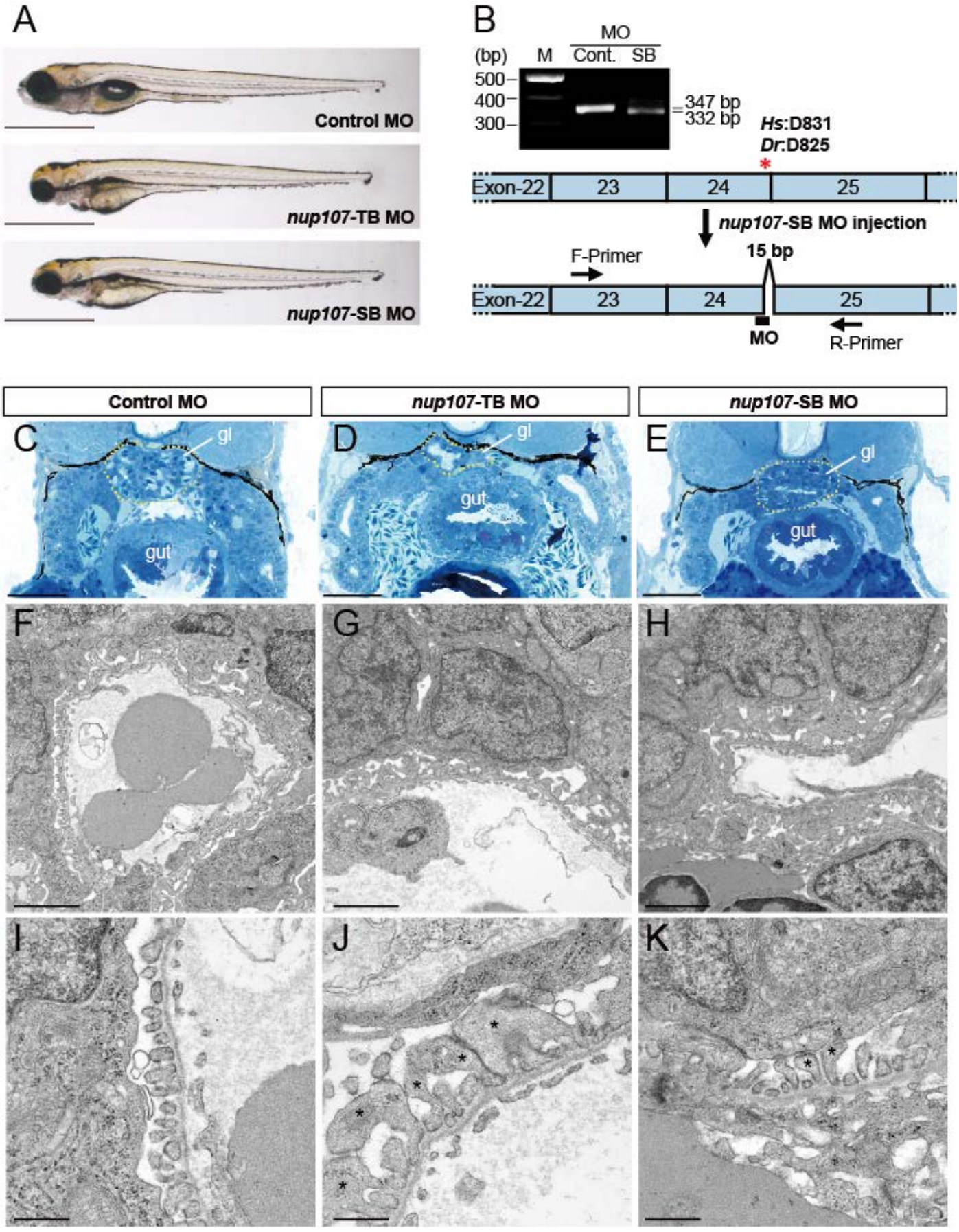

Figure S14. Zebrafish *nup107* Morphant Phenotype Recapitulates the Features of Human SRNS with

***NUP107* Mutations**

(A) Gross morphology of normal and affected larvae injected with control morpholino oligonucleotides (MO), *nup107* translation-blocking MO (*nup107*-TB MO) and *nup107* splice-blocking MO (*nup107*-SB MO). Lateral views of MO-injected larvae at 5 days post-fertilization (dpf) are shown. Scale bars: 1 mm. (B) RT-PCR sequencing of the aberrant splice products show a 15-bp in-frame deletion (WT; 347 bp, *nup107*-SB MO; 332 bp) in the coding exon included a five-amino-acid sequence conserved between humans and zebrafish. The conserved position of the substituted residue in affected individuals (*Homo sapiens*; p.Asp831, *Danio rerio*; p.Asp825) is shown as a red asterisk. The corresponding positions of the F-Primer, R-Primer, and MO are schematically presented. (C-E) Transverse sections of the glomerulus (gl) in the control MO-, *nup107*-TB MO- and *nup107*-SB MO-injected larvae at 5.5 dpf. Scale bars: 0.05 mm. (C) The control MO-injected larvae had a complete glomerular capillary and mesangium. (D) Morphology of the glomerulus and mesangium was markedly disrupted in the *nup107*-TB morphants. (E) The *nup107*-SB morphants showed hypoplastic glomerulus. (F–H) Electron micrographs of the MO-injected larvae at 5.5 dpf. Scale bars: 2 μm. (I–K) electron micrographs at higher magnification. Abnormal shape of the foot processes (asterisks), collapse of the capillary lumen and thickened basement membrane are seen in both *nup107*-TB and *nup107*-SB morphants (G, H, J, K), whereas the control morphant had a normal appearance (F, I). Scale bars: 500 nm.

Figure S15

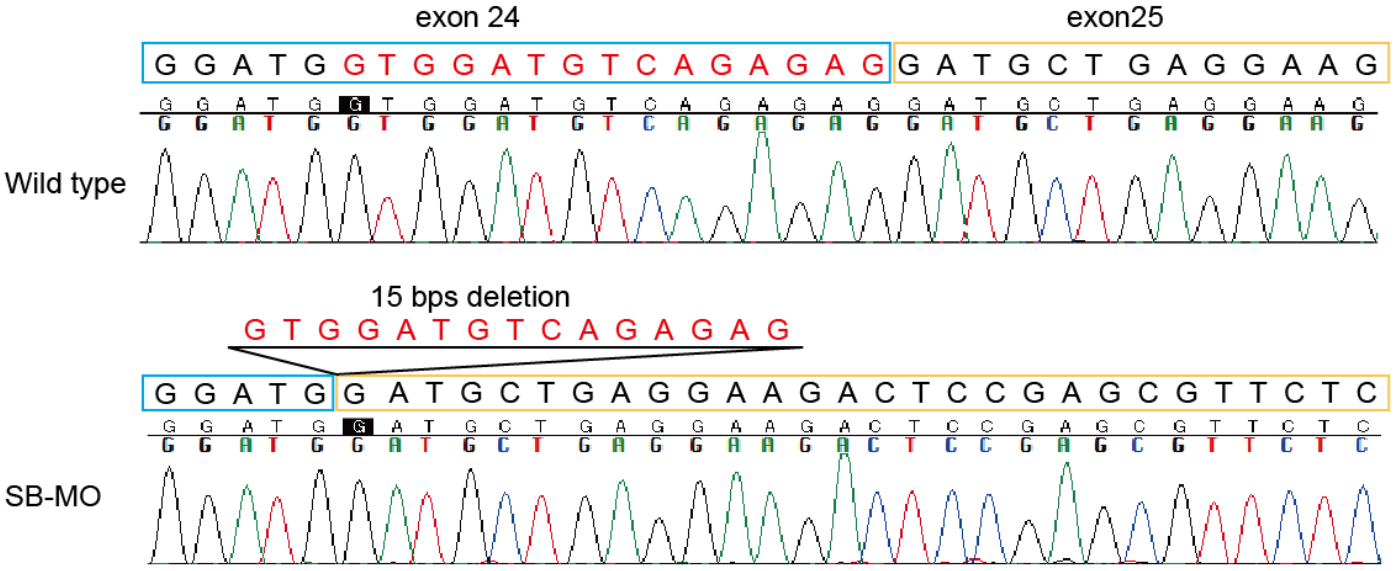

Figure S15. Chromatogram of cDNA sequences in wild-type and SB-MO zebrafish

cDNA sequence of SB-MO shows a 15-bp deletion (red characters) which resulted in an in-frame deletion.

Parts of exons 24 and 25 are indicated by light blue and orange boxes, respectively.

Figure S16

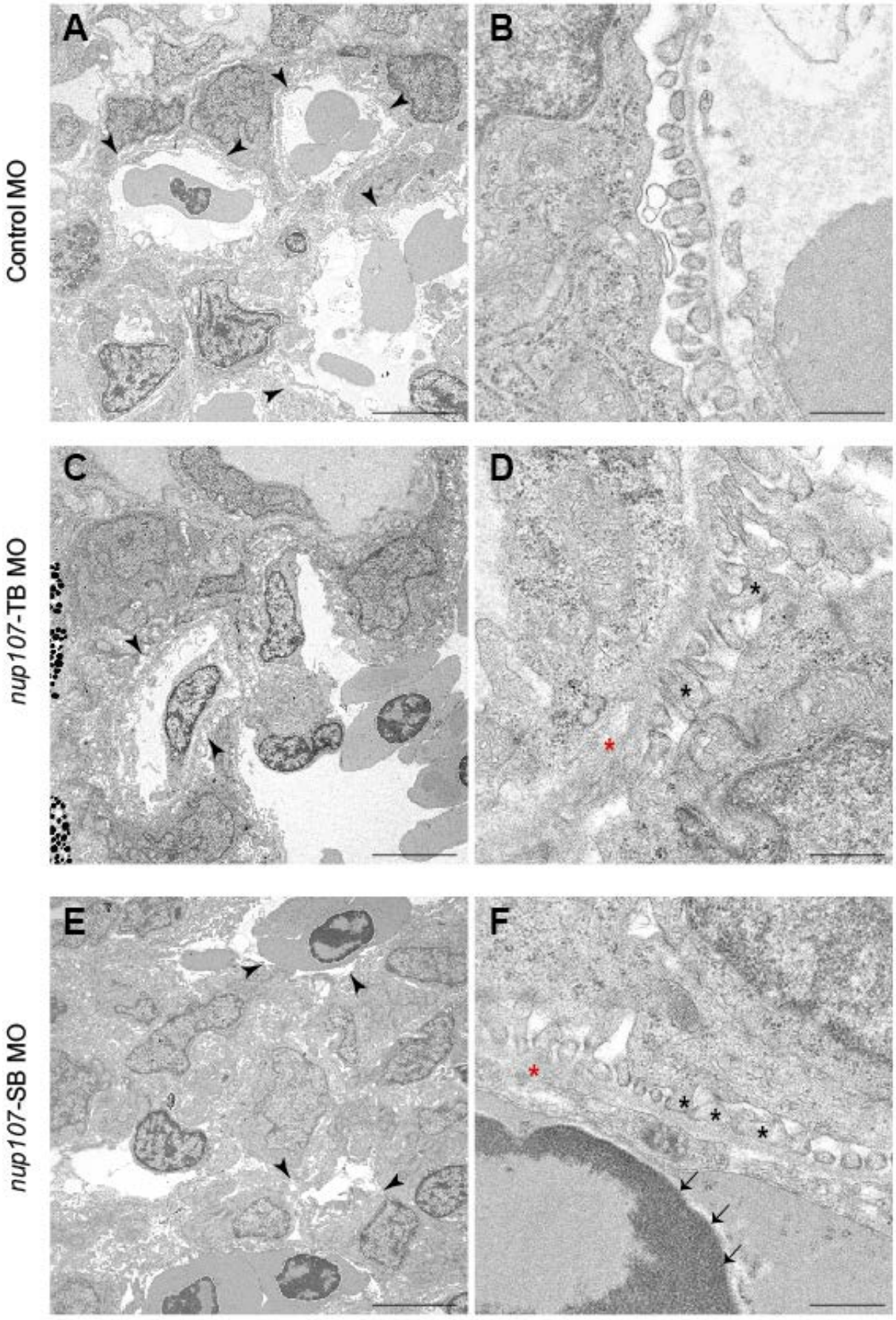

Figure S16. Electron Microscopy of Kidney Samples from Zebrafish *nup107*-Morphants

These electron micrographs depict tissue from the control morphant (A, B), the translation-blocking morphant (*nup107*-TB MO) (C, D), and the *nup107* splice-blocking morphant (*nup107*-SB MO) (E, F). The filtration structures (arrowheads) can be clearly observed in the control morphant (A) but are relatively fuzzy and disorganized in both of the other morphants (C, E). Abnormal foot processes (black asterisks), thickened or blurry basement membranes (red asterisks), and protein droplets (black arrows) could reflect cellular damage in the filtration apparatus. Scale bars: 5 μm (A, C, E); 500 nm (B, D, F).

Figure S17

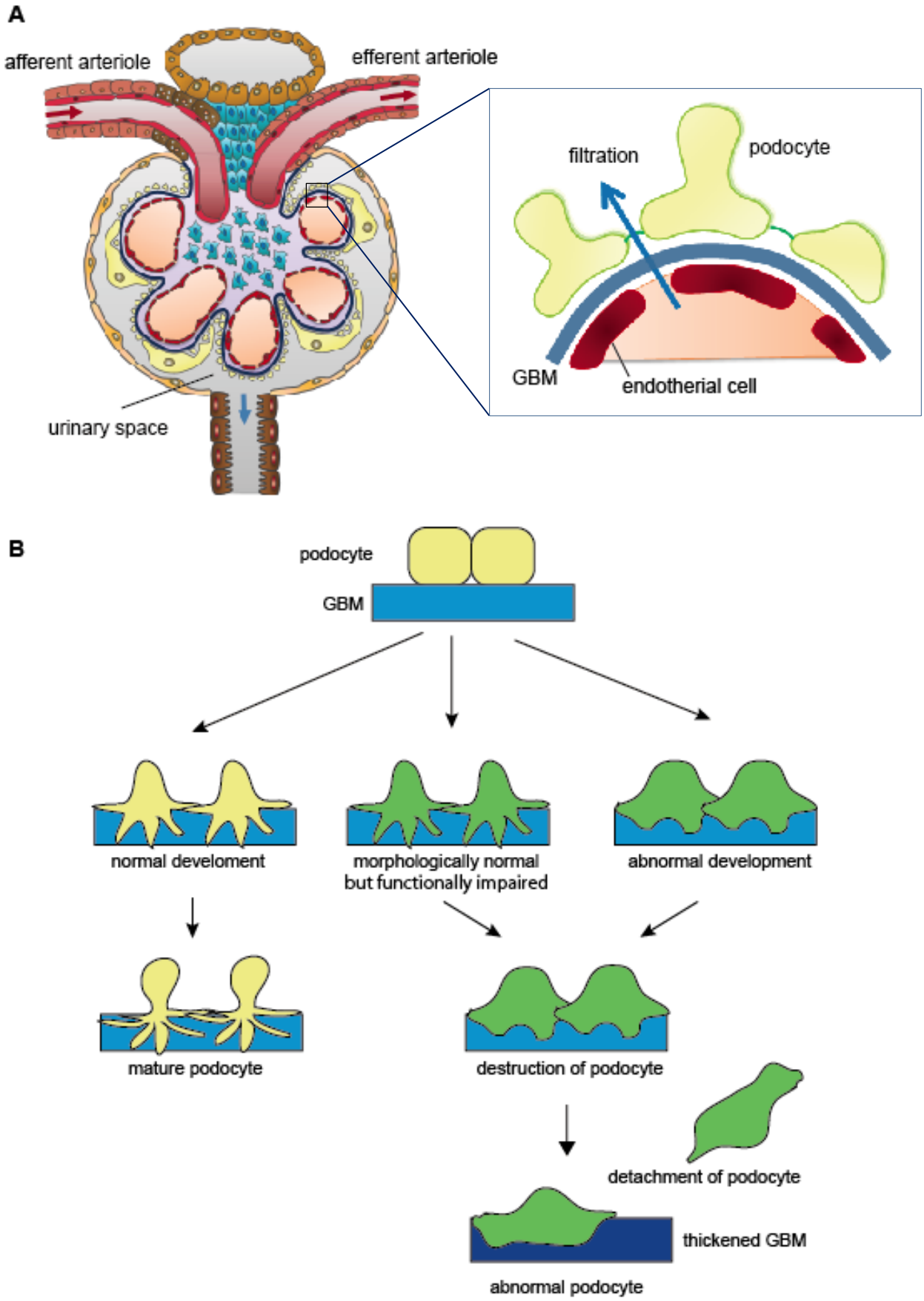

Figure S17. Podocyte Injury Model Based on *NUP107* Mutations

(A) Schematic presentation of the glomerulus. Podocytes (yellow) cover the outer layer of the capillary wall by projecting enormous foot processes with the glomerular basement membrane (dark blue). The inner surface of the capillary lumen is lined with endothelial cells (dark red). The capillary tuft is supported by mesangial cells (light blue) and surrounding matrix (light purple). The enlarged window shows the renal filtration structure. The foot processes of neighboring podocytes (yellow) connect with each other in an interdigitating fashion, leaving 20–50 nm intercellular filtration slits that are bridged by a specialized cell–cell junction known as the slit diaphragm (green line). The slit diaphragm serves as a filtration barrier, which prevents leakage of circulating proteins into the urine. Properly functioning podocytes are crucial for maintaining the integrity and selectivity of the barrier. (B) Podocytes first develop as attached columnar epithelial cells. Attachments between the podocyte cell bodies begin to separate except for the basal part that later forms foot processes through maturation.[3] Normal podocytes (yellow) interact with each other by their foot processes or with the slit membrane, and function as a filter. However, the abnormally developed podocytes (green) possess abnormally fragile foot processes (either by structure or function). As blood pressure increases after birth, the podocytes cannot withstand the post-natal capillary pressure and may become damaged. GBM: glomerular basement membrane.

Table S1. Summary of WES performance (read depth)

Family ID	Individual ID	Identification	Total (bps)	Mean depth	% ≥ 5×	% ≥ 10×	% ≥ 20×
SRNS-1	I-1	Father	2692208251	80.43	97.1	95.8	91.4
SRNS-1	I-2	Mother	2155302585	64.39	96.8	95	88.9
SRNS-1	II-4	Affected individual	2976332475	88.92	97.2	96.1	92.5
SRNS-2	I-2	Mother	1963459760	58.66	96.7	94.6	87.3
SRNS-2	II-1	Affected individual	2941457991	87.88	97.1	95.9	92.3
SRNS-TK1	I-1	Father	2799991123	83.65	97.1	95.8	91.8
SRNS-TK1	I-2	Mother	2322428088	69.38	96.9	95.3	89.9
SRNS-TK1	II-1	Affected individual	3081605879	92.06	97.2	96.2	92.9
SRNS-TWH1	I-1	Father	2506420047	74.88	96.9	95.4	90.4
SRNS-TWH1	I-2	Mother	2930587186	87.55	97	95.8	92.2
SRNS-TWH1	II-1	Affected individual	2698525857	80.62	97	95.7	91.6
SRNS-12	II-3	Affected individual	3210918988	95.93	96.9	95.6	92

Table S2. Priority scheme of homozygous variants in SRNS with *NUP107* mutations

	SRNS-1	SRNS-2	SRNS-TK1	SRNS-TWH1	SRNS-12
Homozygous in affected person as autosome	1139	1111	1136	1103	1120
Non-homozygous in father	153	NA	144	128	NA
Non-homozygous in mother	72	118	75	73	NA
Frequency of ≤ 0.005 in ExAC	19	19	19	19	75
Frequency of ≤ 0.005 in ESP6500	18	19	18	18	68
Frequency of ≤ 0.005 in HGVD	9	8	9	5	47
Frequency of ≤ 0.005 in in-house database	2	1	0	0	0
Non synonymous	1*	0	0	0	0

*The candidate homozygous mutation was listed in Table S4.

Table S3. Priority scheme of compound heterozygous variants in SRNS with *NUP107* mutations

	SRNS-1	SRNS-2	SRNS-TK1	SRNS-TWH1	SRNS-12
Heterozygous variants in affected person as autosome	2343	2146	2047	2089	1903
Non-homozygous in father	2255	NA	1964	1969	NA
Non-homozygous in mother	2144	2059	1861	1890	NA
Frequency of ≤ 0.005 in ExAC	1250	1164	1040	1133	1135
Frequency of ≤ 0.005 in ESP6500	1242	1156	1032	1124	1126
Frequency of ≤ 0.005 in HGVD	680	689	511	561	632
Frequency of ≤ 0.005 in In-house database	412	483	337	374	415
Non synonymous	285	350	229	237	288
Two or more variants in one gene	22	32*	24	20	18*
Compound heterozygous variant (gene)	8 (4)*	NA	6 (3)*	10 (4) *	NA

*The candidates for compound heterozygous variants are listed in Table S5. NA: not analyzed by WES.

Table S6. Mutant Genes Detected in SRNS/FSGS

Gene name	Accession number	MIM	Protein category
ACTN4	NM_004924.4	*604638	Actin cytoskeleton component
ADCK4	NM_024876.3	*615567	Related to CoQ10 synthesis
ANLN	NM_018685.2	*616027	Actin binding protein
APOL1	NM_003661.3	*603743	Secreted high density lipoprotein
ARHGAP24	NM_001025616.2	*610586	RHO GTPase-activating protein
ARHGDIA	NM_001185077.1	*601925	RHO GTPases
CAPN12	NM_144691.3	*608839	Cytosolic calcium-activated cysteine proteases
CD2AP	NM_012120.2	*604241	Slit-Diaphragm protein complex
CFH	NM_000186.3	*134370	Complement factor H
COL4A3	NM_000091.4	*120070	Collagen
COQ2	NM_015697.7	*609825	Mitochondrial protein
INF2	NM_022489.3	*610982	Filament network
LAMA5	NM_005560.3	*601033	Laminin
LAMB2	NM_002292.3	*150325	Glomerular basement membrane
LMNA	NM_170707.3	*150330	Lamin
LMX1B	NM_002316.3	*602575	Nuclear protein
MYH9	NM_002473.4	*160775	Actin cytoskeleton component
MYO1E	NM_004998.3	*601479	Myosin
NPHS1	NM_004646.3	*602716	Slit-Diaphragm protein complex
NPHS2	NM_014625.2	*604766	Slit-Diaphragm protein complex
NXF5	NM_032946.2	*300319	Nuclear RNA export factor 5
PAX2	NM_003987.3	*167409	Transcription factor
PLCE1	NM_016341.3	*608414	Slit-Diaphragm protein complex
PTPRO	NM_030667.2	*600579	Tyrosine phosphatase
SMARCAL1	NM_014140.3	*606622	Nuclear protein
TRPC6	NM_004621.5	*603652	Slit-Diaphragm protein complex
WT1	NM_024426.4	*607102	Nuclear protein

Supplemental References

1. Kitamura, A., Tsukaguchi, H., Iijima, K., Araki, J., Hattori, M., Ikeda, M., Honda, M., Nozu, K., Nakazato, H., Yoshikawa, N., et al. (2006). Genetics and clinical features of 15 Asian families with steroid-resistant nephrotic syndrome. Nephrol Dial Transplant 21, 3133-3138.

2. Boehmer, T., Jeudy, S., Berke, I.C., Schwartz, T.U. (2008). Structural and functional studies of Nup107/Nup133 interaction and its implications for the architecture of the nuclear pore complex. Mol Cell 30, 721-731.

3. Quaggin, S.E., Kreidberg, J.A. (2008). Development of the renal glomerulus: good neighbors and good fences. Development 135, 609-620.